Analytical Methods

ROYAL SOCIETY OF CHEMISTRY

PAPER

View Article Online
View Journal | View Issue

Cite this: *Anal. Methods*, 2026, **18**, 2098

A multimodal approach integrating spectroscopy, deep learning guided molecular docking, and molecular dynamics simulation for predictive assessment of pioglitazone to albumin binding for formulation development

Saswata Banerjee,[a] Sk. Abdul Amin,[b] Shovanlal Gayen,[c] Sakshi Priya,[a] Yashika Tomar,[a] Rajeev Taliyan[a] and Gautam Singhvi *[a]

Binding affinity is a critical parameter that can influence the state of the drug *in vivo* and help to define the formulation strategy. The current study implements a multimodal approach to analyse the binding affinity between human serum albumin (HSA) and pioglitazone. Ultraviolet (UV) absorbance and fluorescence spectrometry analyses were performed on different combinations of HSA and pioglitazone complexes, and the absorbance and fluorescence intensities were mapped to calculate the binding constant. DynamicBind, a distinct deep-learning artificial intelligence tool, was implemented to perform *in silico* docking studies using a non-conventional approach. Furthermore, molecular dynamics simulation was also performed to generate root mean square deviation, radius of gyration, and root mean square fluctuation values, followed by principal component analysis, probability distribution function, and free energy landscape analysis. The simulation output was analysed to interpret the binding affinity and associated conformation of the protein-active pharmaceutical ingredient (API) complex. The binding constant calculated through UV analysis was 1.1×10^4 M^{-1}. Fluorescence spectroscopic analysis derived a value of 1.7×10^5 M^{-1}. At the same time, DynamicBind predicted the cLDDT score for the top predicted model to be 0.634, and a binding affinity value of greater than 5, indicating a relatively moderate binding between pioglitazone and HSA. The results from molecular dynamics simulations further complemented our earlier observations, indicating non-covalent binding interactions and a stable protein-API complex, which is desirable for developing a formulation using HSA as a carrier polymer. This orthogonal approach also provided critical information on the fate of the API and possible considerations that needed to be made during the design of the formulation process, highlighting the need for similar approaches that could provide multifaceted advantages and help in optimising R&D costs and timelines.

Received 13th September 2025
Accepted 1st February 2026

DOI: 10.1039/d5ay01534k

rsc.li/methods

1. Introduction

In the Generic Drug User Fee Act (GDUFA) Fiscal Year 2025 report, the U.S. Food and Drug Administration (USFDA) highlighted the development of orthogonal methods as a key investment area. In previous guidance documents for the characterization of drugs and biologics, the agency has emphasized the need for orthogonal methods as part of additional techniques.[1] This focus is also reflected in ICH guidelines, which have shaped the global understanding of orthogonal and complementary techniques for drug and biologic characterization.[2]

Orthogonal techniques have been critical to elucidate the structural and functional characteristics of drugs and formulations, especially in cases where a single analytical technique is unable to provide a complete dataset. With the advancements in drug formulation and the development of nanomaterials, the emphasis on advanced techniques to characterize individual critical quality attributes (CQAs) has become an area of research interest and is now a crucial part of regulatory submissions. Structure elucidation, drug-polymer binding, and the nature of bonds have also been evaluated in numerous articles and reports.[3–8]

[a]*Industrial Research Laboratory, Department of Pharmacy, Birla Institute of Technology and Science, Pilani, Pilani Campus, Vidya Vihar, Pilani, Rajasthan 333031, India. E-mail: gautam.singhvi@pilani.bits-pilani.ac.in; Tel: +01596-255810*

[b]*Department of Pharmacy, University of Salerno, Via Giovanni Paolo II, 132, 84084 Fisciano, SA, Italy*

[c]*Laboratory of Drug Design and Discovery, Department of Pharmaceutical Technology, Jadavpur University, Kolkata, West Bengal 700032, India*

In the study, we aimed to assess the binding of the pioglitazone drug to human serum albumin (HSA) using two different analytical techniques and two simulation tools. The objective was to verify whether we can use HSA to formulate a polymeric nanoparticle of pioglitazone. HSA nanoparticles have been widely used to increase the solubility of poorly soluble drugs and enhance their pharmacokinetic behaviour *in vivo*.[9–11] They have also been used as a targeted drug delivery system owing to their propensity to be internalized in tumour sites.

The analytical techniques used for the study were UV spectroscopy and fluorescence spectroscopy. Both techniques are spectroscopic in nature but use two different measuring principles. Through our analysis, we tried to determine whether the two analytical techniques can provide comprehensive information on the binding affinity of the drug to HSA, thereby aiding our understanding of the possible *in vivo* behaviour of the formulation.[12,13]

Alongside the two spectroscopic techniques, we performed molecular docking with a deep learning artificial intelligence (AI) docking tool, DynamicBind,[14] and molecular dynamics simulation using Desmond in Schrodinger Release 2021-1, to understand the binding efficiency between HSA and pioglitazone. Previously reported studies considered protein to be of a static nature, which is not the case.[12,13,15,16] In our study, both the simulation tools considered the protein to be in a dynamic state, and the simulation runs took into account the natural motion of the protein and further equilibrated the system to derive the stable conformation, potentially aligning with actual observations.[17,18]

2. Materials & methods

2.1. Materials

Vials containing human serum albumin (20% solution, Grifols) and pioglitazone hydrochloride (gift sample from Dr Reddy's Laboratories Ltd) were used to prepare the diluted albumin-bound pioglitazone nanoparticle. Methanol (Rankem) and acetone (Merck) were used as process solvents to dissolve the poorly soluble pioglitazone HCl. A Jasco V-750 double-beam spectrophotometer was used for UV analysis, and a Horiba Fluorolog 3–21 was employed for fluorescence spectroscopy.

2.2. Methods

2.2.1. Sample preparation. A 12 μM stock solution of HSA was prepared for both spectroscopic techniques. A pioglitazone HCl stock solution was also prepared by dissolving the drug in a 4 : 1 mixture of methanol and acetone to attain a 5 mg mL^{-1} concentration. Next, 2 mL centrifuge tubes were filled with the HSA and pioglitazone stock solutions in different combinations. The pioglitazone concentrations in the centrifuge tubes ranged between 4.45 and 26.7 μg mL^{-1}. The mixtures were vortexed for 1 min and analysed immediately.

2.2.2. UV spectrophotometry analysis. Each sample was analysed using a double-beam UV spectrophotometer (Jasco V-750 spectrophotometer). The blank contained a mixed solution of methanol and acetone. In the sample cuvette, the different API-HSA complexes were transferred and then scanned for absorbance spectra between 200 and 400 nm with data points collected every 1 nm using application software Spectra Manager™. The absorbance and λ_{max} were noted for each complex and HSA alone. The data were next plotted as a double reciprocal graph with absorbance values at 275 nm, with the λ_{max} for HSA alone being used for calculation. Based on the equation for the graph plotted, the binding constant was deduced by dividing the intercept value by the slope value.[15,16]

2.2.3. Fluorospectrometric analysis. Steady-state fluorescence spectroscopy was performed using a Horiba Fluorolog spectrophotometer. An excitation wavelength of 275 nm was applied for both HSA and API–HSA complexes. Using the Horiba Fluorolog spectrophotometer, the emission spectra were analysed for HSA alone and all the combinations of API–HSA complexes. Like UV spectroscopy data, the emission spectra were plotted as a double reciprocal graph with emission values at 361 nm, the emission maximum wavelength for HSA alone. Based on the equation for the graph plotted, the binding constant was deduced by dividing the intercept value by the slope value.

2.2.4. Molecular docking study: DynamicBind simulation. Molecular docking is an important approach for understanding protein-ligand interactions.[19,20] DynamicBind performs dynamic docking by allowing significant protein conformational changes to predict protein-ligand complexes. In this study, the Neurosnap platform was used to perform the AI-based simulation to bind pioglitazone to HSA.[21] The protein structure of HSA (Fig. 1A) was retrieved from the Protein Data Bank (PDB), and the ligand structure (Fig. 1B) was obtained from PubChem. Upon submission of both input parameters in DynamicBind (accessed in the Neurosnap platform on February 18, 2025), docking simulation were performed yielding the top 10 predicted protein-ligand models. The predicted structures were also complemented by their contact-LDDT (cLDDT) scores and binding affinity value, which were generated as part of the algorithm.[14]

2.2.5. Molecular dynamics (MD) simulation study. Molecular dynamics simulation study was performed using the Desmond (D. E. Shaw Research, New York, Academic License, link: https://www.deshawresearch.com/) in Schrodinger Release 2021-1 to understand the dynamic interactive behaviour of the protein-ligand system.[22] As per the standard protocol, the protein-ligand system built up by Desmond software was solvated with the TIP3P water model within a predefined orthorhombic box of 10 Å size. This was followed by neutralization of the charges with an adequate quantity of counterions. Further energy de-escalation was performed by removing steric clashes and other unfavourable interactions. As a final step, the energy-minimized system was loaded for a simulation run for 200 ns at 300 K, with a recording interval of 200 ps as per the NPT ensemble method. Notably, HSA is a single non-glycosylated protein.[23] The output of the simulation runs was next interpreted in terms of the radius of gyration (RG), root-mean square deviation (RMSD), and root-mean square fluctuation (RMSF).[24] Additionally, the free energy landscape (FEL) for the

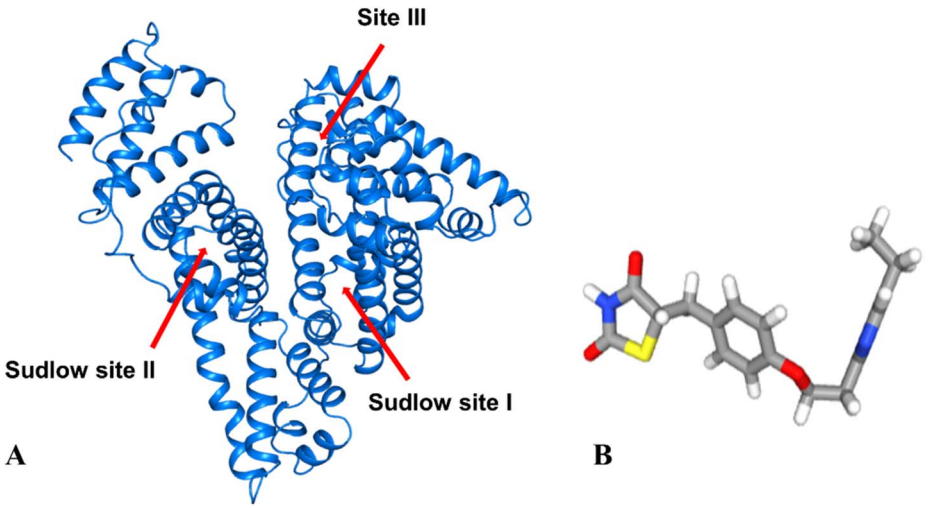

Fig. 1 Structures of (A) human serum albumin (PDB ID 1AO6) and (B) pioglitazone (PubChem CID 4829).

apo protein and protein-ligand complex was next calculated using the Geo-Measures Plugin.[25]

3. Results & discussion

For macromolecules like HSA, fluorescence behaviour can help early researchers to understand the molecular interaction between molecules of interest and HSA. Parameters that can be ascertained through fluorescence studies include binding affinity, the binding mechanism, and the ligand binding site on the protein. Spectroscopic studies have played a significant role in annotating this behaviour. It has also been used to interpret the conformational changes the protein undergoes for binding to the protein.[12,15,16,23,26–29]

HSA is a 585 amino acid monomeric protein consisting of 17 disulfide bridges, with its secondary structure chiefly composed of α-helices. HSA (Fig. 1A) consists of 9 loops, spanning three homologous domains named Domain I (residues 1-195), II (residues 196-383), and III (residues 384-585), with each domain consisting of two long and one short loop. Each domain is further divided into two subdomains, with the first two loops denoted as subdomain A, and the remaining being denoted as subdomain B. HSA contains 35 cysteine residues, of which all, except the C34 residue in Domain I, are involved in a disulfide bond, further stabilizing the protein structure. Although these homologous domains appear to have similar structures, each domain exhibits distinct binding characteristics.[23,30–33]

It contains two major drug-binding sites: Sudlow site I (subdomain IIA), which preferentially binds bulky heterocyclic compounds, and Sudlow site II (subdomain IIIA), which favors aromatic compounds. In addition, a third major non-Sudlow binding site has been identified in subdomain IB, capable of accommodating a wide range of endogenous and exogenous ligands. Albumin also possesses up to seven binding sites for long-chain fatty acids, each with distinct binding affinities.[33]

In the present study, subdomain IIA (Sudlow site I) is of particular interest because pioglitazone contains a 2,4-thiazolidinedione ring and a pyridine moiety, structural features that favour binding at this site. HSA exhibits intrinsic fluorescence arising from three amino acid residues (tryptophan, tyrosine, and phenylalanine). Among these, tryptophan is the dominant fluorophore, and Sudlow site I is enriched with the key residue W214. The fluorescence contribution of phenylalanine is minimal, while tyrosine fluorescence is often diminished due to ionization and interactions with neighbouring amino and carboxyl groups, including proximity to tryptophan. Consequently, fluorescence quenching experiments primarily probe interactions involving W214 in subdomain IIA, enabling precise characterization of ligand binding at Sudlow site I.[12,34] Additionally, binding of small molecule drugs may not fill the hydrophobic pocket of the Sudlow site I, thereby predisposing the site to be filled with water molecules, and further hydrogen bond interaction with the polar residues at the site.[33,35]

3.1. UV spectrophotometry analysis

UV spectroscopic analysis is a simple and effective process to qualitatively and quantitatively measure the binding nature between the protein and ligand. UV analysis of HSA alone revealed a λ_{max} at 275 nm. Further analysis of the HSA-drug complexes revealed a blueshift of the UV spectrum (Fig. 2). This indicated an interaction between the amino acids in the hydrophobic pocket and those of pioglitazone. The hypsochromic spectrum shift is predominantly associated with the structural changes that the protein undergoes to accommodate the ligand at its preferred binding site. This phenomenon has been widely reported in multiple literature studies and can be considered a cornerstone for structural analysis of protein-ligand complexes.[15,16,30] Besides the shift in the UV spectrum, a proportional increase in absorption intensity was also observed. An increase in intensity with an increase in drug concentration could also be attributed to the presence of pioglitazone. Pioglitazone has a λ_{max} of 265 nm.[35,36] In general, the presence of a ligand accentuates the blueshift, but in this specific case, it also contributes to the absorption intensity for

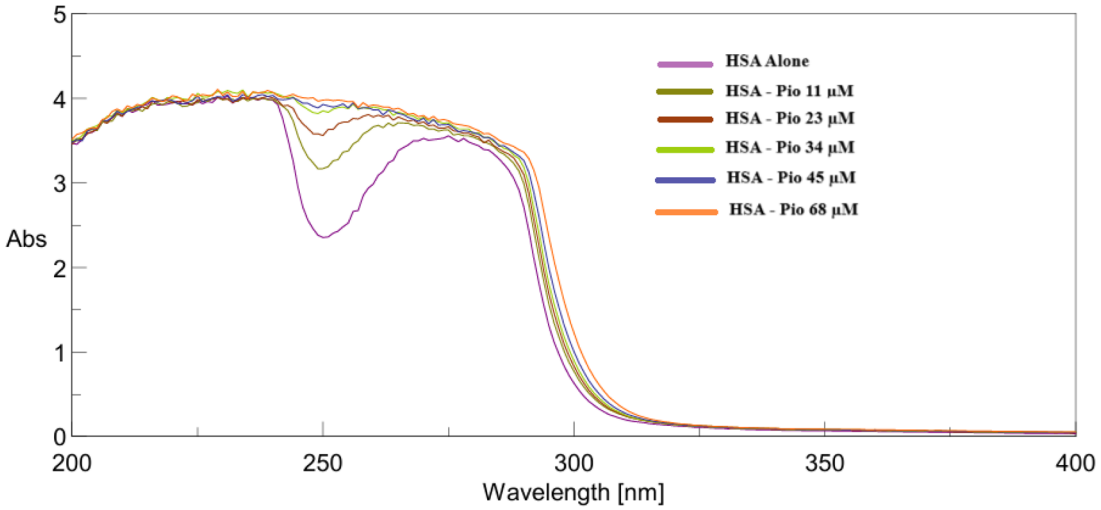

Fig. 2 The overlay of the UV spectra shows the hypsochromic shift of the absorbance for the different samples, with the λ_{max} shifting to shorter wavelengths with increasing concentration and higher absorbance.

the drug–protein complexes. The increase in intensity due to higher concentrations of the drug can indicate that the drug itself did not undergo any change and was able to hold on to its functional groups. It may also point to the fact that the binding of pioglitazone to the amino acid residues is non-covalent and the occurrence of a π–π transition with the tryptophan residues at the binding site.[19]

3.2. Fluorospectrometric analysis

The fluorometric analysis involves quantifying photoluminescence triggered by the absorption of UV wavelengths. As previously established, HSA exhibits known photoluminescence properties, primarily due to the presence of tryptophan residues. A spectroscopic analysis of HSA alone revealed that an excitation wavelength of 275 nm at room temperature generated an emission spectrum with a λ_{max} at 361 nm. Like UV spectroscopy, fluorometric analysis generated emission spectra for individual drug-HSA complexes and a similar hypsochromic shift (Fig. 3). On the other hand, the emission intensity showed a behaviour opposite to that of UV spectroscopy. Pioglitazone does not possess any fluorophore and hence did not contribute to the fluorescence intensity. The decline in intensity can be attributed to the utilization of tryptophan residues and adjacent amino acid residues for binding to pioglitazone. The inverse relationship proved the preferred binding site to be Sudlow site I for pioglitazone.[37–40]

3.3. Double-reciprocal graphs to determine the binding constant

A double reciprocal graph with respect to pioglitazone molar concentration was plotted to determine the binding constant. For UV spectroscopy (Fig. 4), the mode values of $1/(A_0 - A)$ were

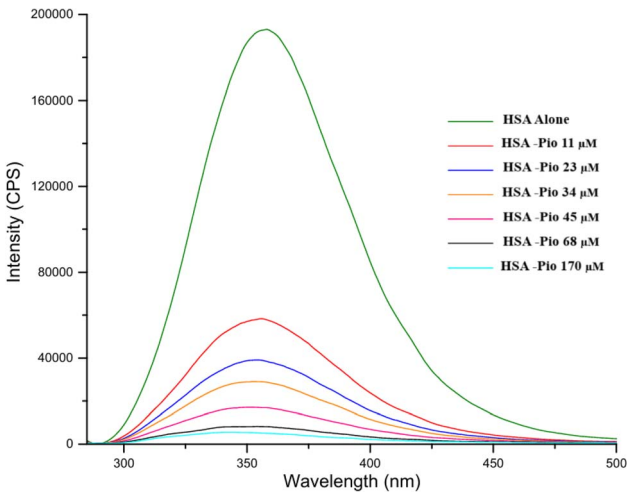

Fig. 3 The overlay of the emission spectra shows the hypsochromic shift of the fluorescence for the different samples, with the emission maximum shifting to shorter wavelengths with increasing concentration and lower fluorescence.

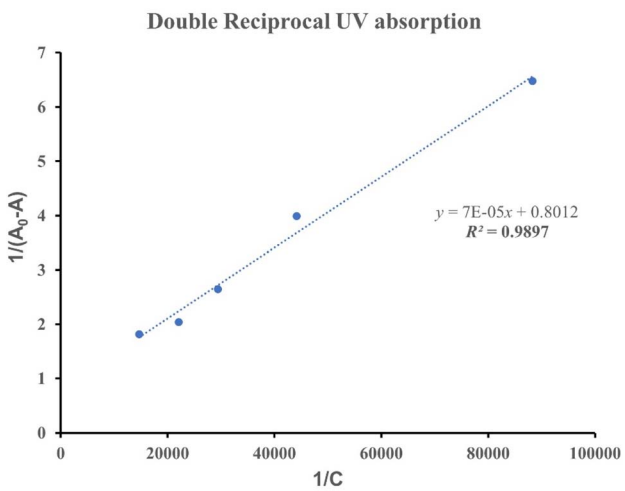

Fig. 4 The double reciprocal graph of UV absorbance with different HSA-pioglitazone complexes.

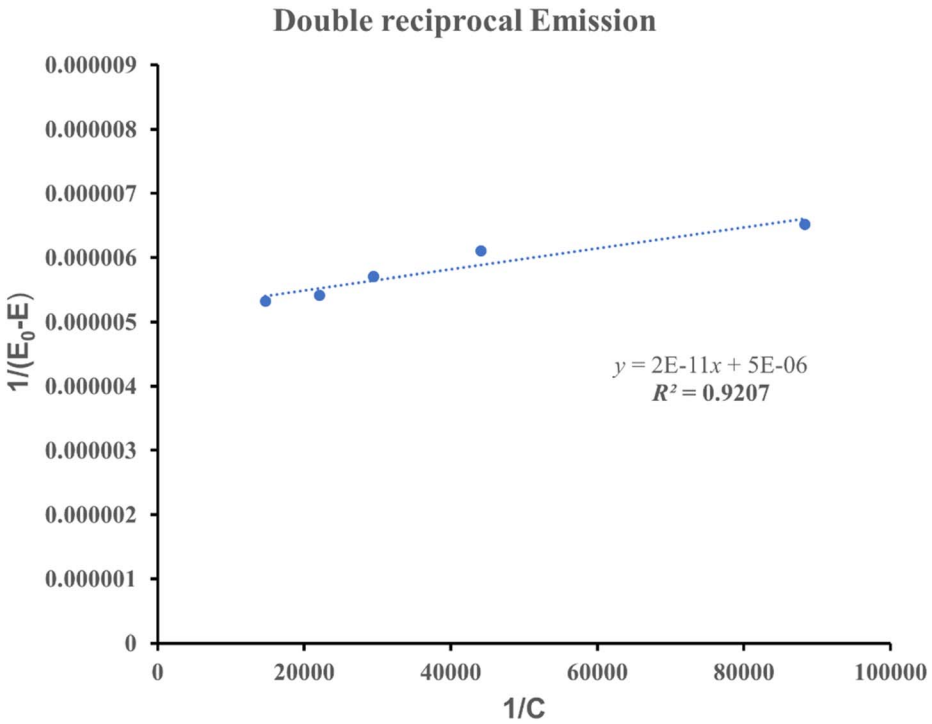

Fig. 5 The double reciprocal graph of fluorescence emission with different HSA-pioglitazone complexes.

considered for plotting the graph and plotted with regard to the inverse of the molar concentration of pioglitazone in the samples. For fluorescence spectroscopy (Fig. 5), the $1/(E_0 - E)$ values were plotted *vs.* the reciprocal of pioglitazone molar concentration of the samples. In the respective cases, A_0 and E_0 indicated the absorbance for HSA alone at 275 nm and the emission of HSA alone at an emission wavelength of 361 nm. The spectroscopic titration by individual methods was performed for individual concentrations at the aforementioned wavelengths for the respective methods. For fluorescence spectroscopic titration, an emission/fluorescence correction (E_{cor}) was performed, considering the inner filter effect study, as per eqn (1), where absorbance values of pioglitazone at excitation (A_{ex}) and emission (A_{em}) wavelengths were considered for the correction E_{obs}.[41]

$$E_{cor} = E_{obs} \times 10^{\frac{A_{ex}}{2} + \frac{A_{em}}{2}} \quad (1)$$

The plotted graph showcased a linear relationship with a correlation coefficient higher than 0.9 for both spectroscopic procedures. The binding constant derived from the graph was next calculated by dividing the intercept value by the slope of the graph. The binding constant calculated through UV analysis had a value of 1.1×10^4 M^{-1}, while fluorescence spectroscopic analysis derived a value of 1.7×10^5 M^{-1}. Both these values are indicative of medium affinity (expected values to be between 10^3 and 10^6 M^{-1}).[12,15,16,37,39]

The binding affinity of a drug to the protein site can influence its therapeutic effectiveness *in vivo*. The ability of a drug to diffuse from systemic circulation and reach its intended target depends much on its binding affinity to plasma proteins like HSA. Our study aimed to evaluate the binding affinity and nature of interactions of pioglitazone with HSA. A drug weakly bonded to HSA will have poor bioavailability as it will be poorly distributed, rapidly metabolised, and eliminated, thereby having a shorter half-life. Strongly bonded drugs, in contrast, will not be efficiently released to be available, resulting in subtherapeutic effectiveness. Moderately bonded drugs ensure that the drug will efficiently diffuse through the biological barrier and have the required half-life to be transported through the systemic circulation to its intended activity site. At the same time, the affinity does not impede its release, thereby ensuring the availability of the drug in sufficient concentration to exert its therapeutic impact. The binding affinity values generated through orthogonal studies complement the understanding with regard to the values derived from spectroscopic measurements.[15,16,30,38]

3.4. DynamicBind simulation

DynamicBind is a geometric deep generative model that considers proteins not to be in a state of rigid configuration while docking.[14] The ability of proteins to transition between multiple conformations is central to their functional character *in vivo*. Ligands, especially drug moieties, can only bind to specific conformations of the targeted protein molecule, thereby regulating the overall impact of the drug in the biological system. It outperforms other models in predicting possible ligand poses for known protein datasets (PDB and MDT). It does so by being able to predict protein configurations with lower Root Mean Square Deviation (RMSD) scores for regions around the binding sites, providing a protein conformation resembling its native state. The cLDDT scoring

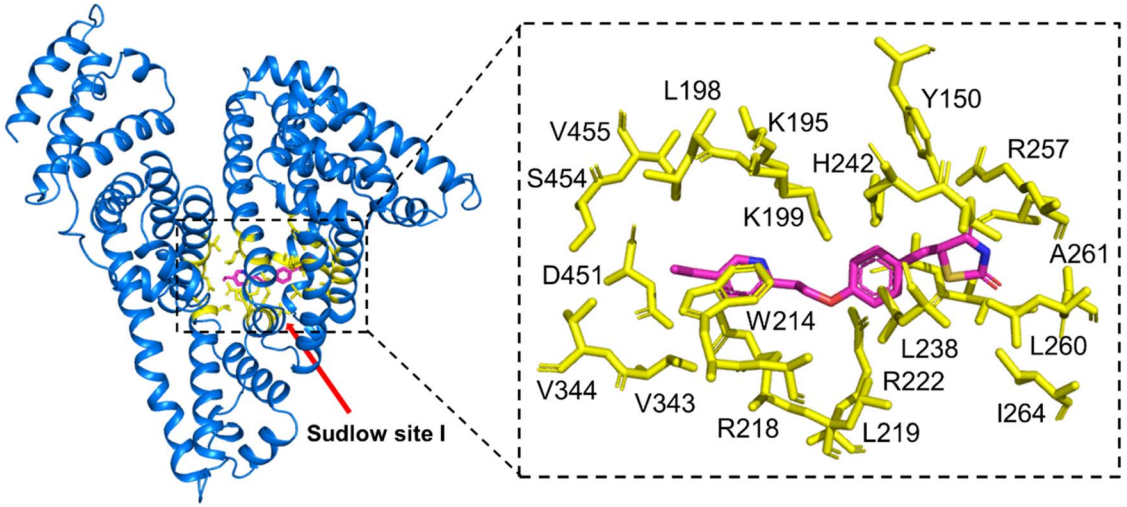

Fig. 6 Possible binding mode of pioglitazone (shown as a pink stick model) within the binding site of human serum albumin (HSA, shown as a cartoon representation). Interacting residues are highlighted in yellow.

developed as a measuring parameter for DynamicBind generated models is well aligned with the auROC score, showing its effectiveness in selecting the most appropriate model from amongst its multiple predicted protein-ligand complexes. DynamicBind also calculates binding affinity as a negative logarithm value of dissociation and complements the cLDDT score to assess the quality of ligand interaction with the protein binding site.[14,42]

DynamicBind predicted the cLDDT score for the top predicted model to be 0.634, with the range varying for the top model between 0.634 and 0.472, with the absolute value of 1 indicative of near native contact.[21] A binding affinity value greater than 5 indicates a relatively moderate binding between pioglitazone and HSA.[43] The results are consistent with the practical observations from the spectroscopy analysis, where we predicted the affinity to be of medium intensity. Therefore, DynamicBind can serve as a usable tool for initial screening and understanding. The fact that it demands far less computational power compared to conventional docking tools makes it lucrative for researchers working on early-stage projects.

Aside from the binding interaction deduced through spectroscopic analysis, the simulated docking study also identified

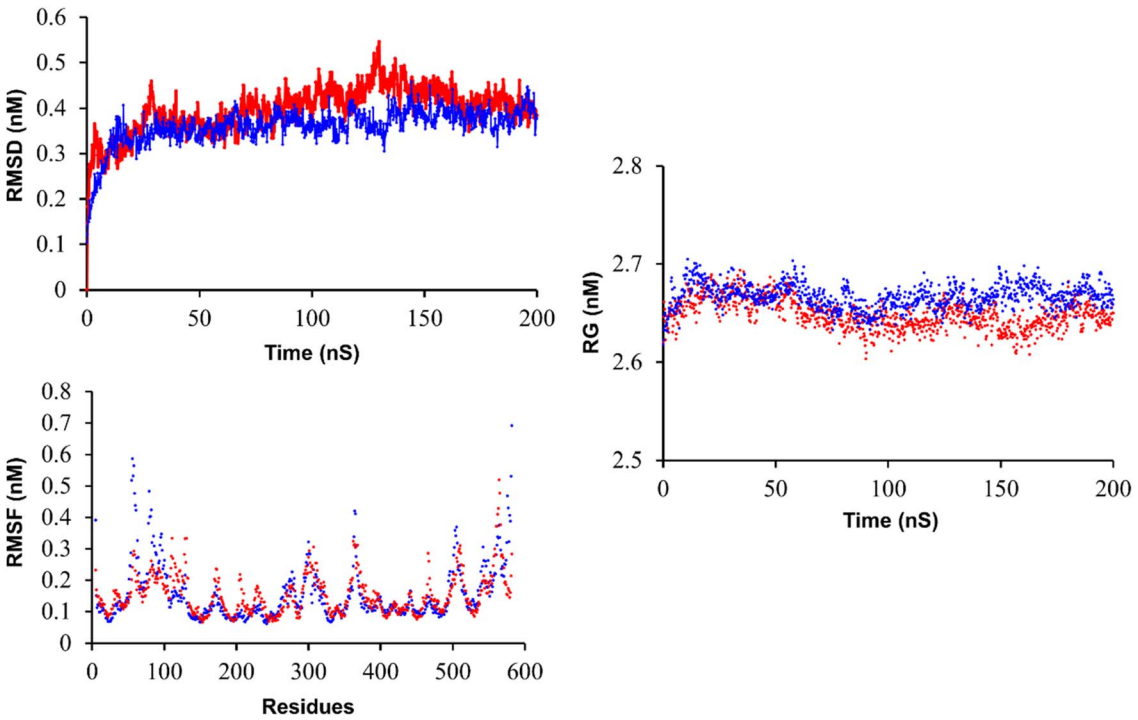

Fig. 7 Comparison of RMSD, RMSF, and RG of apo-human serum albumin (blue) and its complexes with pioglitazone (red).

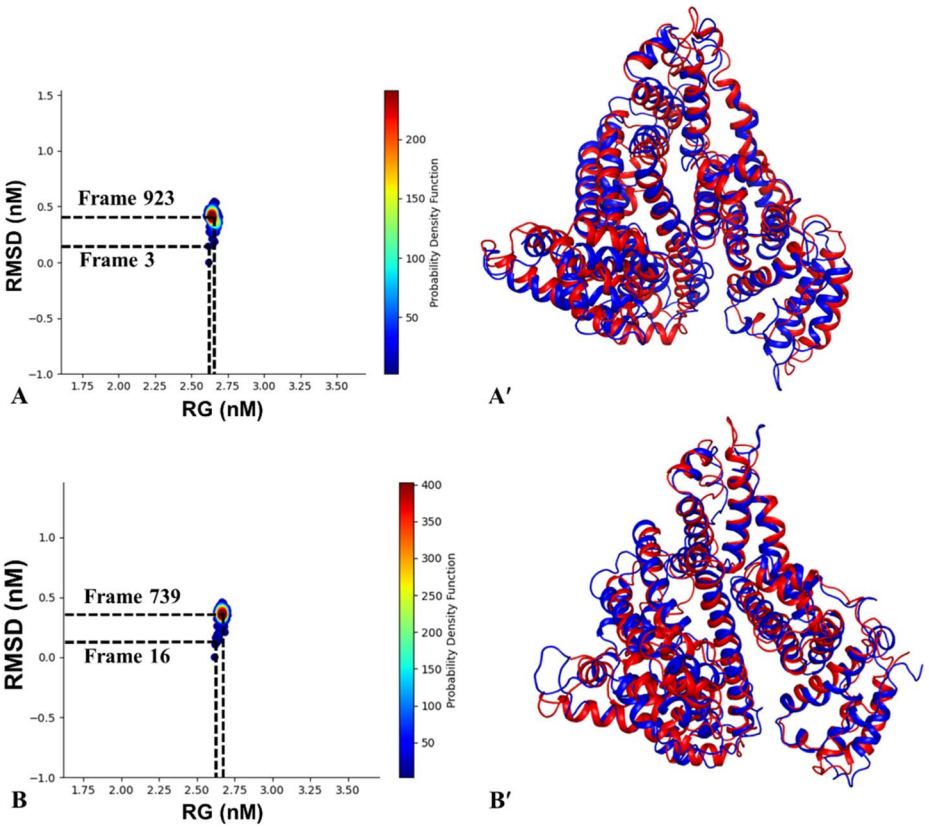

Fig. 8 Probability density function (PDF) plot along with the corresponding largest (blue), sparsely populated (red) conformation in the case of apo-HSA (A, and A') and pioglitazone-bound HSA (B, and B').

other interactions and their nature. A π–π stacked interaction is evident between the pyridine ring and the tryptophan residue (W214), with the electron-rich indole ring of tryptophan contributing to such non-covalent interactions, inadvertently stabilizing the protein-ligand system (Fig. 6).

A π-alkyl interaction between W214 and the alkyl chain adjacent to pyridine is also predicted, owing again to the indole group of W214.[44,45] The other predicted interaction involving amino acid residues other than W214 includes a π-cation interaction of the pyridine ring of pioglitazone with the arginine residue (R218) owing to the positively charged guanidinium group,[46] a π-alkyl interaction between the benzene ring of pioglitazone and the leucine residue (L238), and a hydrogen bond between the R257 residue and the thiazolidinedione ring (Fig. S1). The possible nature of binding interactions is thereby non-covalent, further supporting our earlier assumptions derived from the previously executed studies.

3.5. Molecular dynamics (MD) simulation study

The molecular dynamics simulation was run for a period of 200 ns, and the stability of the protein-API system was assessed. The assessment was done on the RG, RMSD, and RMSF values derived for the protein in both the apo and bound states. The RMSD values, as observed from Fig. 7, indicate that the protein-ligand system is as stable as the apo-protein structure, while the RG values for both protein systems show similar compactness, corroborating the previous observation obtained through DynamicBind simulation. The residual mobility of the bounded and unbounded form of human serum albumin was further computed, and the resulting RMSF values for the residue seem to be comparable with those of the apo protein, showing more structural flexibility than the bounded form.[47,48]

Hydrogen-bond analysis of the MD trajectory revealed stable and persistent interactions between pioglitazone and key HSA residues. R257 exhibited the highest hydrogen-bond occupancy (~77%), followed by S287 (~34%) and R222 (~16%), indicating their critical roles in ligand stabilization. Additional hydrogen-bond interactions were observed with R218 (~13%), L260 (~8%), and A261 (~1%). As shown in Fig. S2, the timeline analysis illustrates the dynamic evolution of pioglitazone-HSA interactions, highlighting both the overall interaction frequency and residue-wise contact persistence throughout the simulation. Collectively, the high occupancy and temporal stability of these hydrogen bonds support the favourable binding orientation of pioglitazone and confirm the dynamic stability of the pioglitazone-HSA complex during the MD simulation.

3.6. Probability density function (PDF) analysis

The probability density function plots analysed the different conformations of the apo and ligand-bound protein. They mapped them based on the highest (in blue) and lowest (in red)

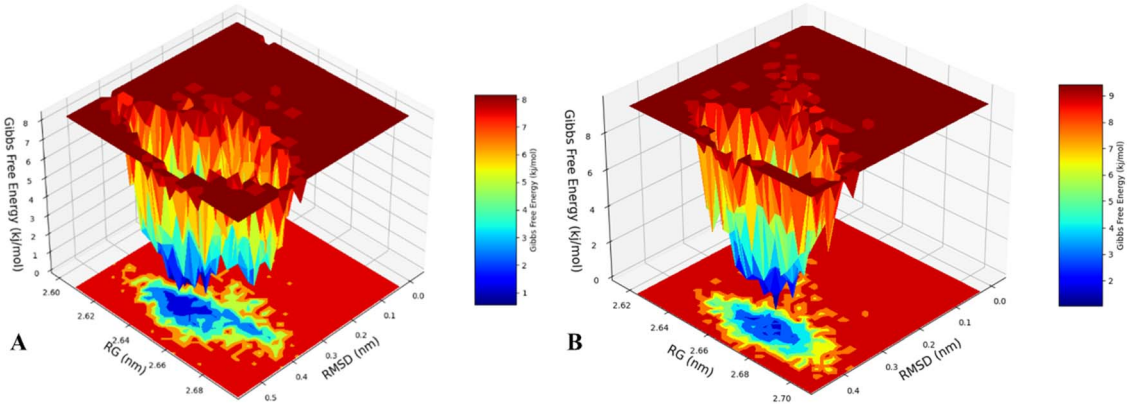

Fig. 9 Free energy landscape (FEL) plot of (A) apo-HSA and (B) pioglitazone-bound HSA.

occurring conformations (Fig. 8). The differences in the RMSD value between the highest and lowest conformers for both the apo protein seemed to be higher than that of the ligand-bound protein, indicating a higher flexibility for the unbound protein than that of the bound protein. In the case of RG values, the differences between the highest and lowest conformers of the apo-protein seem to be narrower than those for the API bound protein, indicating structural changes and slight relaxation of the protein secondary structure.[47,49]

3.7. 3D Free Energy Landscape (FEL) analysis

The 3D FEL plots (Fig. 9) were prepared to map the free energy variation in accordance with the RMSD and RG values for different conformations of the unbound (apo) and bound protein conformations. The 3D plot for the apo protein showcased a wider cluster of low-energy peaks, which may be a result of multiple conformations being in a metastable state, owing to the absence of a ligand to restrict the apo protein to a stable conformer (Fig. 9A). On the other hand, a narrow cluster of low-energy peaks was derived for the API-bound protein complex, indicating a more stable conformation (Fig. 9B). The observations were comparable to those observed through PDF analysis and further demonstrate the correlation between RMSD and RG values with free energy variation, to deduce conformer stability.[47,49]

3.8. Principal component analysis (PCA)

Furthermore, principal component analysis of the MD trajectory data was performed to account for any alteration in the major global atomic motion of amino acid residues in unbound

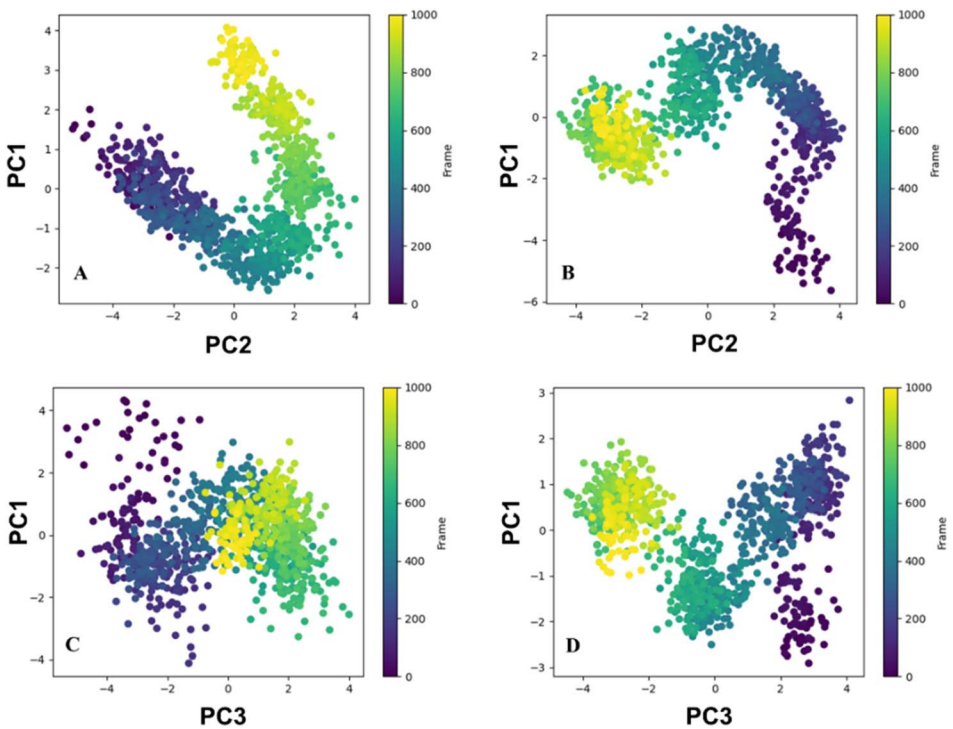

Fig. 10 PCA plot for [A/C] for HSA and [B/D] for pioglitazone-bound HSA.

(apo) and bound HSA. The coherent internal 3D motions were captured using a covariance matrix, with the resulting eigenvectors representing dominant modes of motion in the trajectory. Notable differences in trajectory clustering were observed for both the unbound (apo) and bound proteins (Fig. 10).

In the case of apo-HSA, all intermediate frames (excluding initial frames) clustered along PC1 *vs.* PC2, indicating global conformational shifts. Interestingly, the terminal frames (800–1000) of the pioglitazone-bound HSA complex scattered together, suggesting a trend toward convergence, unlike the more dispersed apo structure. Meanwhile, in the PC1 *vs.* PC3 projection, the terminal apo-HSA frames aligned along PC3, indicating subtle side-chain rearrangements (Fig. 10). These shifts likely reflect the presence of multiple low-energy conformers, consistent with findings from previous FEL analyses (Fig. 9).

4. Conclusion

In this study, we tried to assess the implementation of a few simple techniques to determine the tested parameter. The spectroscopic techniques discussed include commonly available instruments. Compared with advanced tools such as nuclear magnetic resonance, our approaches require simpler sample preparation, instrument handling, and data interpretation, making them more feasible for early-stage researchers. Notably, this study employed a deep learning-based artificial intelligence framework to perform non-conventional, dynamic molecular docking. In contrast to similar types of previously reported studies[40,50] that typically treat HSA as rigid entities, the present work considers the HSA in a dynamic state during docking. Furthermore, the use of DynamicBind *via* the user-friendly Neurosnap platform eliminates the need for high-performance computing resources, thereby broadening accessibility to the wider research community. Complementary 200 ns molecular dynamics simulations provided additional insights into binding efficiency, protein-ligand complex stability, and conformational behavior, collectively strengthening the reliability and mechanistic interpretation of the results.

The understanding derived is pivotal for designing the formulation strategy and predicting probable behaviour of the formulated product involving HSA as a carrier for pioglitazone *in vivo*. The moderate binding affinity values of pioglitazone to HSA, derived through spectroscopic techniques, further corroborated to an extent by the simulation tools, provided affirmative proof of the suitability for developing an HSA-bound formulation system. The spectroscopic analysis and docking study indicated that the binding between the drug and protein is non-covalent and exhibits the requisite affinity, which is expected to improve the drug's bioavailability. The simulated docking studies further shed light on a possible formulation pathway. The cLDDT score suggests that for the interaction to occur, a slight modification is required in the native protein conformation. These findings indicate that incorporating an energy-input step into the process design may facilitate binding. Therefore, through this pre-formulation study, which aimed to determine the binding affinity *via* an orthogonal approach, we derived information that could help us design the process and predict *in vivo* behavior. This can also prove beneficial as it will help reduce R & D cost and timeline, showing the utility of orthogonal techniques beyond regulatory stipulations.

Author contributions

Saswata Banerjee: conceptualization, methodology, investigation, data curation, formal analysis, writing – original draft, visualization. Sk. Abdul Amin: investigation, data curation, formal analysis, writing – original draft, visualization. Shovanlal Gayen: data curation, formal analysis, writing – original draft, supervision. Sakshi Priya: data curation, writing – review & editing. Yashika Tomar: data curation, writing – review & editing. Rajeev Taliyan: writing – review & editing, supervision. Gautam Singhvi: writing – review & editing, supervision.

Conflicts of interest

There are no conflicts of interest to declare.

Data availability

The authors confirm that the data supporting the findings of this study are available within the article [and/or] its supplementary information (SI). Supplementary information is available. See DOI: https://doi.org/10.1039/d5ay01534k.

Acknowledgements

This research did not receive any specific grant from funding agencies in the public, commercial, or not-for-profit sectors. This research received no external funding. The authors would like to thank and acknowledge the Central Instrument Facility, BITS Pilani, Pilani campus, for allowing the use of its facilities and for providing access to the UV spectrophotometer and spectrofluorometer for analysis purposes. We sincerely acknowledge the Department of Pharmacy, University of Salerno, Italy, and the Department of Pharmaceutical Technology, Jadavpur University, India, for providing the research facilities.

References

1 U.S. Food and Drug Administration. FY 2025 GDUFA Science and Research Priority Initiatives. https://www.fda.gov/drugs/generic-drugs/fy-2025-gdufa-science-and-research-priorities. Accessed on February 2026.
2 International Council for Harmonisation of Technical Requirements for Pharmaceuticals for Human Use (ICH). Validation of Analytical Procedures Q2(R2). https://database.ich.org/sites/default/files/ICH_Q2-R2_Document_Step2_Guideline_2022_0324.pdf Accessed on February 2026.

3 C. G. Simon, S. E. Borgos, L. Calzolai, B. C. Nelson, J. Parot, E. J. Petersen, M. X. Roesslein and F. Caputo, Orthogonal and complementary measurements of properties of drug products containing nanomaterials, *J. Controlled Release*, 2023, **354**, 120–127.
4 E. Van Gyseghem, S. Van Hemelryck, M. Daszykowski, F. Questier, D. L. Massart and Y. Vander Heyden, Determining orthogonal chromatographic systems prior to the development of methods to characterise impurities in drug substances, *J. Chromatogr. A*, 2003, **988**(1), 77–93.
5 K. M. Tyner, N. Zheng, S. Choi, *et al.*, How Has CDER Prepared for the Nano Revolution? A Review of Risk Assessment, Regulatory Research, and Guidance Activities, *AAPS J.*, 2017, **19**, 1071–1083.
6 F. Caputo, J. Clogston, L. Calzolai, M. Rösslein and A. Prina-Mello, Measuring particle size distribution of nanoparticle enabled medicinal products, the joint view of EUNCL and NCI-NCL. A step by step approach combining orthogonal measurements with increasing complexity, *J. Contr. Release*, 2019, **299**, 31–43.
7 L. Newey-Keane. The Power Of Orthogonality In Assessing The Stability Of Biopharmaceuticals. https://www.technologynetworks.com/analysis/news/the-power-of-orthogonality-in-assessing-the-stability-of-biopharmaceuticals-211659 Accessed on February 2026.
8 Yokogawa Fluid Imaging Technologies, Inc. Enhancing biotherapeutic research: The role of orthogonal and complementary analytical techniques. https://www.news-medical.net/whitepaper/20240718/Enhancing-biotherapeutic-research-The-role-of-orthogonal-and-complementary-analytical-techniques.aspx Accessed on February 2026.
9 S. Tayyab and S. R. Feroz, Serum albumin: clinical significance of drug binding and development as drug delivery vehicle, *Adv. Protein Chem. Struct. Biol.*, 2021, **123**, 193–218.
10 A. B. Gurung, M. A. Ali, J. Lee, M. A. Farah, K. M. Al-Anazi and H. Sami, Molecular modelling studies unveil potential binding sites on human serum albumin for selected experimental and *in silico* COVID-19 drug candidate molecules, *Saudi J. Biol. Sci.*, 2022, **29**(1), 53–64.
11 H. Y. Tao, R. Q. Wang, W. J. Sheng and Y. S. Zhen, The development of human serum albumin-based drugs and relevant fusion proteins for cancer therapy, *Int. J. Biol. Macromol.*, 2021, **187**, 24–34.
12 H. Gao, L. Lei, J. Liu, Q. Kong, X. Chen and Z. Hu, The study on the interaction between human serum albumin and a new reagent with antitumour activity by spectrophotometric methods, *J. Photochem. Photobiol., A*, 2004, **167**(2–3), 213–221.
13 A. A. Salem, M. Lotfy, A. Amin and M. A. Ghattas, Characterization of human serum albumin's interactions with safranal and crocin using multi-spectroscopic and molecular docking techniques, *Biochem. Biophys. Rep.*, 2019, **20**, 100670, DOI: 10.1016/j.bbrep.2019.100670.
14 W. Lu, J. Zhang, W. Huang, Z. Zhang, X. Jia, Z. Wang, L. Shi, C. Li, P. G. Wolynes and S. Zheng, DynamicBind: predicting ligand-specific protein-ligand complex structure with a deep equivariant generative model, *Nat. Commun.*, 2024, **15**(1), 1071.
15 A. Najmi, M. Albratty, H. A. Alhazmi, N. Thangavel, M. S. Alam, W. Ahsan, S. A. Javed, I. A. Arbab and K. A. El-Sharkawy, Spectroscopic and *in silico* approach to probe the binding interactions of irbesartan and human serum albumin, *J. King Saud Univ. Sci.*, 2022, **34**(3), 101875.
16 M. A. Bratty, Spectroscopic and molecular docking studies for characterizing binding mechanism and conformational changes of human serum albumin upon interaction with Telmisartan, *Saudi Pharm. J.*, 2020, **28**(6), 729–736.
17 T. Sakano, M. I. Mahamood, T. Yamashita and H. Fujitani, Molecular dynamics analysis to evaluate docking pose prediction, *Biophys. Physicobiol.*, 2016, **13**, 181–194.
18 D. Gioia, M. Bertazzo, M. Recanatini, M. Masetti and A. Cavalli, Dynamic docking: a paradigm shift in computational drug discovery, *Molecules*, 2017, **22**(11), 2029.
19 Y. Yue, Q. Tu, Y. Guo, Y. Wang, Y. Xu, Y. Zhang and J. Liu, Comparison of the interactions of fanetizole with pepsin and trypsin: spectroscopic and molecular docking approach, *J. Mol. Liq.*, 2022, **365**, 120095.
20 X. Wang, Y. Yue, Y. Zhang, Z. Wang, J. Liu and Q. Tang, Probing the interaction of pepsin with imidacloprid *via* DFT calculation, spectroscopic approaches and molecular docking, *J. Mol. Struct.*, 2019, **1197**, 210–216.
21 Neurosnap Inc. - Computational Biology Platform for Research. Wilmington, D.E., 2022. https://neurosnap.ai/. Accessed on February 2026.
22 K. J. Bowers, E. Chow, H. Xu, R. O. Dror, M. P. Eastwood, B. A. Gregersen, & D. E. Shaw, Scalable algorithms for molecular dynamics simulations on commodity clusters, in *Proceedings of the 2006 ACM/IEEE Conference on Supercomputing*, p. , p. 84-es.
23 P. Lee and X. Wu, Modifications of human serum albumin and their binding effect, *Curr. Pharm. Des.*, 2015, **21**(14), 1862–1865.
24 S. Khatun, R. Islam, S. A. Amin, A. Bhattacharya, D. K. Dhaked, T. Jha and S. Gayen, Nitrogen-containing heterocycles as an important scaffold for selective and potent HDAC8 inhibition: a step towards effective, non-toxic and selective HDAC8 inhibitor discovery, *J. Biomol. Struct. Dyn.*, 2024, 1–19.
25 L. P. Kagami, G. M. das Neves, L. F. S. M. Timmers, R. A. Caceres and V. L. Eifler-Lima, Geo-Measures: a PyMOL plugin for protein structure ensembles analysis, *Comput. Biol. Chem.*, 2020, **87**, 107322.
26 A. Szkudlarek, Effect of palmitic acid on tertiary structure of glycated human serum albumin, *Processes*, 2023, **11**(9), 2746.
27 S. A. Mardikasari, G. Katona and I. Csóka, Serum albumin in nasal drug delivery systems: exploring the role and application, *Pharmaceutics*, 2024, **16**(10), 1322.
28 R. Vaidyanathan, S. M. Sreedevi, K. Ravichandran, S. M. Vinod, Y. H. Krishnan, L. K. Babu and V. Mahalingam, Molecular docking approach on the binding stability of derivatives of phenolic acids (DPAs) with Human Serum Albumin (HSA): hydrogen-bonding

versus hydrophobic interactions or combined influences?, *J. Colloid Interface Sci. Open*, 2023, **12**, 100096.
29 M. Bteich, An overview of albumin and alpha-1-acid glycoprotein main characteristics: highlighting the roles of amino acids in binding kinetics and molecular interactions, *Heliyon*, 2019, **5**(11), e02879.
30 X. Q. Zhou, B. L. Wang, S. B. Kou, Z. Y. Lin, Y. Y. Lou, K. L. Zhou and J. H. Shi, Multi-spectroscopic approaches combined with theoretical calculation to explore the intermolecular interaction of telmisartan with bovine serum albumin, *Chem. Phys.*, 2019, **522**, 285–293.
31 S. Curry, Lessons from the crystallographic analysis of small molecule binding to human serum albumin, *Drug Metabol. Pharmacokinet.*, 2009, **24**(4), 342–357.
32 A. Sułkowska, Interaction of drugs with bovine and human serum albumin, *J. Mol. Struct.*, 2002, **614**(1–3), 227–232.
33 S. Sugio, A. Kashima, S. Mochizuki, M. Noda and K. Kobayashi, Crystal structure of human serum albumin at 2.5 Å resolution, *Protein Eng.*, 2009, **12**(6), 439–446.
34 National Center for Biotechnology Information, *PubChem Compound Summary for CID 4829*, Pioglitazone, 2025. https://pubchem.ncbi.nlm.nih.gov/compound/Pioglitazone. Retrieved on February 23, 2025.
35 S. Imre, D. Anghel, A. Puşcaş, A. G. Cârje, D. L. Muntean, A. Balint and C. Toma, Contributions to quality control by HPLC of fixed combinations with pioglitazone and metformin, *Acta Med. Transilv.*, 2023, **28**(2), 11–16.
36 United States Pharmacopoeia, *Pioglitazone and Metformin Hydrochloride Tablets Monograph. USP 40-NF 35*, 2016, Accessed on February 2026.
37 V. Rajendiran, R. Karthik, M. Palaniandavar, V. S. Periasamy, M. A. Akbarsha and B. S. Srinag, Mixed-ligand copper(II)-phenolate complexes: effect of coligand on enhanced DNA and protein binding, DNA cleavage, and anticancer activity, *Inorg. Chem.*, 2007, **46**, 8208–8221.
38 C. Dufour and O. Dangles, Flavonoid-serum albumin complexation: determination of binding constants and binding sites by fluorescence spectroscopy, *BBA*, 2004, **1721**, 164–173.
39 J. Li, J. Li, Y. Jiao and C. Dong, Spectroscopic analysis and molecular modeling on the interaction of jatrorrhizine with human serum albumin (HSA), *Spectrochim. Acta, Part A*, 2014, **118**, 48–54.
40 F. Faridbod, M. R. Ganjali, B. Larijani, S. Riahi, A. A. Saboury, M. Hosseini and C. Pillip, Interaction study of pioglitazone with albumin by fluorescence spectroscopy and molecular docking, *Spectrochim. Acta, Part A*, 2011, **78**(1), 96–101.
41 Y. Yue, Y. Wang, Q. Tu, Y. Xu, Y. Zhang, Q. Tang and J. Liu, A comprehensive insight into the effects of punicalagin on pepsin: Multispectroscopy and simulations methods, *J. Mol. Liq.*, 2022, **365**, 120194.
42 F. Wong, A. Krishnan, E. J. Zheng, H. Stärk, A. L. Manson, A. M. Earl and J. J. Collins, Benchmarking AlphaFold-enabled molecular docking predictions for antibiotic discovery, *Mol. Syst. Biol.*, 2022, **18**(9), e11081.
43 Y. Wang, Y. Zhou and F. I. Khan, Molecular Insights into Structural Dynamics and Binding Interactions of Selected Inhibitors Targeting SARS-CoV-2 Main Protease, *Int. J. Mol. Sci.*, 2024, **25**(24), 13cors482.
44 W. Li, S. Huang, H. Wen, Y. Luo, J. Cheng, Z. Jia and W. Xue, Pyridine functionalized carbon dots for specific detection of tryptophan in human serum samples and living cells, *Microchem. J.*, 2020, **154**, 104579.
45 S. Marincean, M. Al-Modhafir and D. B. Lawson, π-π stacking interactions in tryptophan-lumiflavin-tyrosine: a structural model for riboflavin insertion into riboflavin-binding protein, *J. Mol. Model.*, 2025, **31**(2), 38.
46 D. A. Dougherty, Cation-π interactions involving aromatic amino acids, *J. Nutr.*, 2007, **137**(6), 1504S–1508S.
47 S. Dawn, P. Manna, T. Das, P. Kumar, M. Ray, S. Gayen and S. A. Amin, Exploring fingerprints for antidiabetic therapeutics related to peroxisome proliferator-activated receptor gamma (PPARγ) modulators: A chemometric modeling approach, *Comput. Biol. Chem.*, 2024, **112**, 108142.
48 S. Khatun, I. Dasgupta, S. Sen, S. A. Amin, I. A. Qureshi, T. Jha and S. Gayen, Histone deacetylase 8 in focus: Decoding structural prerequisites for innovative epigenetic intervention beyond hydroxamates, *Int. J. Biol. Macromol.*, 2025, **284**, 138119.
49 A. Bhattacharjee, S. Kar and P. K. Ojha, Unveiling G-protein coupled receptor kinase-5 inhibitors for chronic degenerative diseases: Multilayered prioritization employing explainable machine learning-driven multi-class QSAR, ligand-based pharmacophore and free energy-inspired molecular simulation, *Int. J. Biol. Macromol.*, 2024, **269**, 131784.
50 S. Sharmeen, A. Woolfork and D. S. Hage, Generation of affinity maps for thiazolidinediones with human serum albumin using affinity microcolumns. I. Studies of effects by glycation on multisite drug binding, *J. Chromatogr. B*, 2024, **1236**, 124070.

